EXAFS measurements of liquid Se-Te mixtures

1991 J. Phys.: Condens. Matter 3 7495

(http://iopscience.iop.org/0953-8984/3/38/021)

J. Phys.: Condens. Matter 3 (1991) 7495–7510. Printed in the UK

EXAFS measurements of liquid Se–Te mixtures

K Tamura†, M Inui‡, M Yao§, H Endo§, S Hosokawa†, H Hoshino‖, Y Katayama§* and K Maruyama§

† Faculty of Integrated Arts and Sciences, Hiroshima University, Hiroshima 730, Japan
‡ College of General Education, Kyushu University, Fukuoka 810, Japan
§ Department of Physics, Faculty of Science, Kyoto University, Kyoto 606, Japan
‖ Faculty of Education, Hirosaki University, Hirosaki 036, Japan

Received 23 April 1991

Abstract. We have measured EXAFS spectra of liquid(l-) Se, Te, Se–Te mixtures and vapour (v-) Se for the first time. It is clearly observed that the two-fold coordinated chain structure is largely preserved in l-Se and that the intrachain covalent bond contracts on melting. The EXAFS spectra of l-Te can be reproduced well by assuming a two-fold coordinated chain structure with shorter and longer bonds within the chain. In order to obtain partial structure-parameters in liquid Se–Te mixtures, spectra are taken on both Se and Te K edges. The Se–Se bond elongates with increasing Te concentration. The number of the longer Te–Te bonds increases with increasing temperature or increasing Te concentration; this may be associated with the semiconductor-to-metal transition.

1. Introduction

It has been reported that the two-fold coordination in the chain of crystalline Se (c-Se) is largely preserved on melting [1, 2], and that liquid Te (l-Te) has a three-fold coordinated structure [3–6]. However, in l-Te there are serious disagreements about the interpretation of the first peak in the radial distribution function because the first coordination shell substantially overlaps the second. Recently Enderby and Barnes [7] have suggested that the covalently bonded chain structure may be preserved even in l-Te, and that one of the three neighbouring atoms has a distinct bond origin.

Liquid Se (l-Se) exhibits semiconducting behaviour similar to that of c-Se, while l-Te exhibits metallic behaviour. Recent measurements of various physical properties for liquid Se–Te mixtures such as density [8, 9], sound velocity [10, 11], specific heat [12], electrical conductivity [13–15], magnetic susceptibility [16–18], NMR [18, 19] and optical properties [20, 21] show that a semiconductor-to-metal transition is induced by raising the temperature or by increasing the Te concentration. It is suggested that the transition is accompanied by a structural transformation from the liquid Se-like structure to the liquid Te-like one. However, the partial distribution functions of liquid Se–Te mixtures have not been obtained.

EXAFS measurements give useful information on the local environment around central Se and Te atoms in the mixtures. In particular, EXAFS has an advantage in that it can extract information on the intrachain atomic arrangements, since the EXAFS signals due to the interchain correlation are expected to be damped in the liquid state. This is due

* Present address: Faculty of Science and Technology, Keio University, Yokohama 223, Japan

0953-8984/91/387495 + 16 $03.50

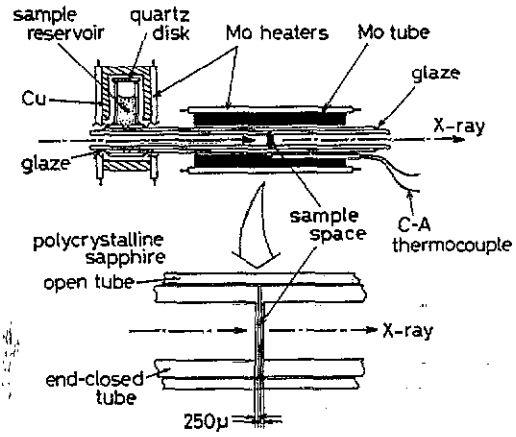

Figure 1. The construction of the sapphire cell used for EXAFS measurements with an enlargement showing the sample space.

to disorder and thermal agitation [22]. There has been little application of the EXAFS technique to liquids at high temperature [22–25] because it is difficult to keep a thin liquid sample stable in a cell. We have measured EXAFS of l-Se, Te, Se–Te mixtures and v-Se for the first time by using polycrystalline sapphire cells of our own design. Since the wave-vector dependence of the photoelectron backward scattering amplitude of a Se atom is very different from that of Te, clear separation of the data into the scattering originating from Se and Te atoms is possible. We have succeeded in deducing the partial structure-parameters of the first coordination shell in the mixtures.

2. Experimental technique

EXAFS experiments for l-Se, Te and Se–Te mixtures were performed using the spectrometer installed at BL-10B of the Photon Factory in the National Laboratory for High Energy Physics (KEK). With a silicon (311) channel-cut monochromator, an energy resolution of 1.1 eV at 9 keV was achieved with a typical photon flux of 10^9 photons s^{-1} when the storage ring was operated at 2.5 GeV and 300 mA [26]. The reproducibility of the energy axis was better than 0.0005 deg; this corresponds to 0.3 eV around the Se K-edge and 2 eV around the Te K-edge. The intensity of the incident beam I_0 and the transmitted beam I were monitored using two ionization chambers filled with 85%–15% nitrogen–argon mixtures and pure argon for the Se K-edge, and with pure argon and pure krypton for the Te K-edge. X-ray absorption spectra were measured over the range from 12.4 to 13.8 keV for the Se K-edge and from 31.5 to 33.0 keV for the Te K-edge. The integration time for photon counting above the Te K-edge was 10 s per point; this is ten times as long as that above the Se K-edge because of the low photon flux. In a typical run, it took 20 min to survey the region around the Se K-edge, and 100 min around the Te K-edge.

In order to deduce the EXAFS oscillation $\chi(k)$ as a function of photoelectron wave-vector k, the background level for higher shells and the absorption of an isolated atom were subtracted from the observed absorption $\ln(I_0/I)$ using the Victoreen fit and cubic spline technique [27]. The subtracted spectrum was then normalized by the absorption of an isolated atom to obtain $\chi(k)$. For the measurements of EXAFS for l-Se, Te and Se–Te mixtures (which have a high vapour pressure and a highly corrosive nature) we have developed a sample cell made of polycrystalline sapphire. The cell assembly is illustrated in figure 1. Two sapphire tubes with outer diameters of 6.5 mm and inner

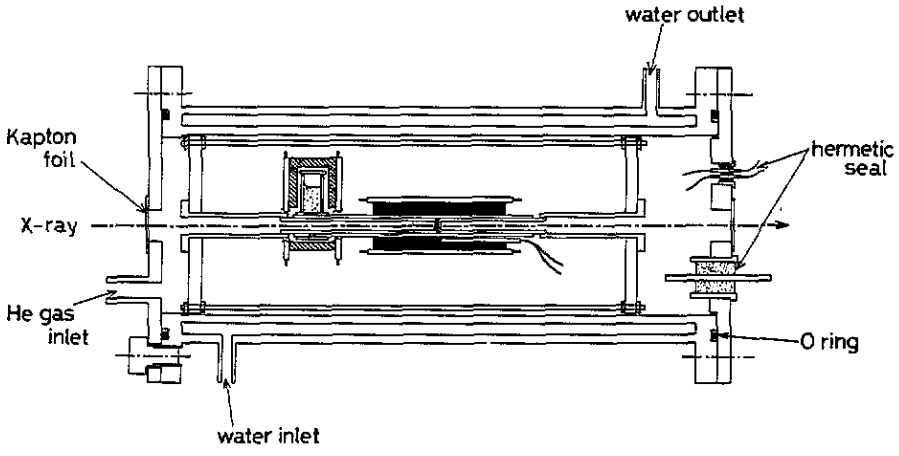

Figure 2. A side view of the cylindrical water-cooled chamber for EXAFS measurements.

diameters of 4.0 mm were prepared. The length of the longer tube was 40 mm and the shorter one 30 mm. Each of the tubes had one closed end. These tubes were inserted into another open tube having an inner diameter of 6.5 mm, an outer diameter of 8.0 mm and a length of 65 mm, in such a way that the closed ends of the inner tubes faced each other with a narrow and uniform gap between them. The closed ends were polished to a thickness of 250 μm in order to improve the efficiency of x-ray transmission. The thickness of the sample space was adjusted so that the jump in the x-ray absorption at the absorption edge, $\Delta\mu t$, was about 1. The thickness was from 40 μm to 200 μm for liquid samples and 20 mm for Se vapour. It is useful to note that, when a single crystal sapphire cell was used, we observed spurious peaks in the EXAFS spectrum due to the Bragg reflections from the cell. In the present experiment, therefore, we used polycrystalline sapphire with a grain size smaller than 15 μm. As shown in the figure, the sapphire components were cemented together with high temperature glaze (Owen–Illinois Inc Type 01328–C).

The cell was heated by a heating element made of molybdenum (Mo) wire. As seen in the figure the Mo heater was set around a Mo tube which kept the temperature of the sample space uniform. The temperature was measured by chromel–alumel thermocouples which were inserted into the holes drilled in the Mo tube and were in close contact with the sapphire wall in the vicinity of sample space. The sample reservoir was maintained at a temperature about 50 °C above the melting point of the sample during the EXAFS measurements. The reservoir was encased with copper which trapped the Se and Te vapour escaping from the reservoir.

The sample cell was positioned in a cylindrical water-cooled chamber with x-ray windows of Kapton. Figure 2 shows the side view of the chamber. As indicated in the figure, the x-ray beam passed through the Kapton windows, the closed-ends of sapphire tubes and the liquid sample. The collimation of the x-ray beam was performed by using x and z translation stages on which the chamber was fixed.

The sample space was filled with the liquid sample in the following way. First, the chamber was evacuated and the sample space was heated to a temperature around 500 °C. Then, the chalcogen sample loaded in the reservoir was fused by heating it to a temperature 50 °C above the melting point. Finally, He gas at atmospheric pressure was introduced into the chamber to force the fused sample to the sample space through a

narrow channel between the outer and inner sapphire tubes. It was confirmed by means of x-ray photography that the liquid sample filled up the sample space completely. The gaseous state sample was prepared by heating the sample space above the boiling point while maintaining the temperature of the reservoir near the melting point.

For the measurements of l-Te in the supercooled state, a quartz cell similar to the sapphire cell was used. The cell filled with Te was put into a furnace with x-ray windows. After raising the temperature above the melting point, the furnace was cooled slowly down to temperatures below the melting point. We determined the freezing point by monitoring the density change from x-ray absorption measurement. For the measurements of c-Se and Te at 80 K and room temperature, solid samples were powdered and sandwiched between two layers of Scotch tape. EXAFS spectra on c-Se at high temperatures were measured using a graphite cell.

3. Results and discussion

3.1. Liquid Se

Figure 3 shows EXAFS oscillations $\chi(k)$ of c-, l- and v-Se at various temperatures. The pattern of $\chi(k)$ of l-Se is similar to that of c-Se. The amplitude of $\chi(k)$ has a peak around 7 Å^{-1} and it becomes smaller with increasing temperature. The data for v-Se at 1473 K, a much higher temperature than the boiling point, show rather simple oscillations compared with data obtained near the boiling point.

Figure 4 shows the magnitude of the Fourier transform, $|F(r)|$, of $\chi(k)$ multiplied by k for c-, l- and v-Se. The first sharp peak of c-Se at 80 K corresponds to the distribution of the intrachain nearest neighbour atoms. The second peak consists of two peaks—one corresponds to that of the interchain nearest neighbours and the other the intrachain second nearest neighbours. Distributions of interchain second neighbours and intrachain third neighbours appear in the third peak. In the $|F(r)|$ at 300 K, the first peak is still sharp but the second peak is reduced. At 478 K just below the melting point the second peak disappears, suggesting large fluctuations in the interchain distance and in the bond angle. When Se is melted, the first peak is shifted towards smaller r. The peak of l-Se at 523 K is nearly as high as that of c-Se at 478 K, implying that the coordination number of l-Se is 2, as it is for c-Se. With increasing temperature the peak height becomes lower, while the position is almost unchanged. The first peak of v-Se lies at a much smaller distance than that of l-Se. This means that the bond of v-Se is stronger than that of l-Se, which is consistent with the fact that the vapour consists of Se_2 dimers [28].

In order to determine the structural parameters such as bond length r_1 and the mean square displacement σ_1 we have used the standard technique of Fourier filtering. In this analysis the first peak in $|F(r)|$ of Se was back-transformed into k-space. The resulting Fourier filtered spectrum $\tilde{\chi}(k)$ was fitted with the following formula.

$$k^2\tilde{\chi}(k) = SB_{Se}(k')k'N_1 \exp(-2k'^2\sigma_1^2)\frac{\sin(2k'r_1 + \varphi_{Se}(k'))}{r_1^2} \tag{1}$$

$$k' = (k^2 - \Delta E_0/3.81)^{1/2}. \tag{2}$$

Here $B_{Se}(k)$ and $\varphi_{Se}(k)$ are the backward scattering amplitude and phase shift functions of Se. We used $B_{Se}(k)$ and $\varphi_{Se}(k)$ as calculated by McKale *et al* [29].

In the curve fitting procedure, the scaling factor S, the ratio of the experimental amplitude to the calculated one, was selected to be 0.65; this gives 2 as the coordination

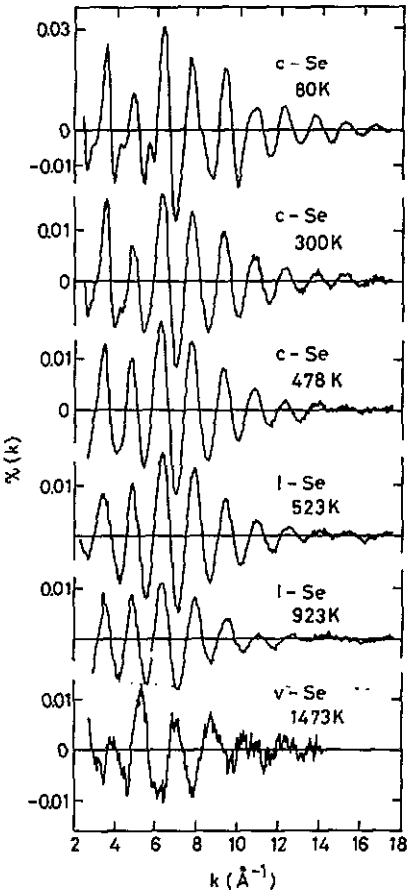

Figure 3. The EXAFS oscillation $\chi(k)$ of c-, l- and v-Se at various temperatures.

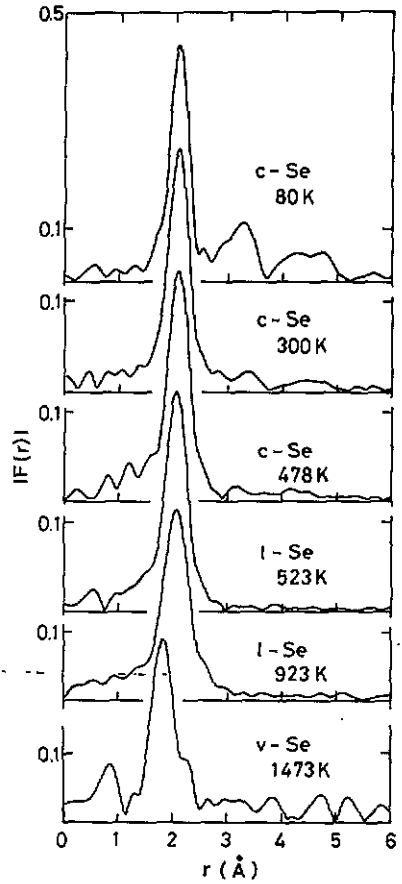

Figure 4. The magnitude of Fourier transform, $|F(r)|$, of k times $\chi(k)$ in figure 3.

number N_1 of c-Se. We also adopted a reasonable assumption that N_1 is 2 for l-Se and 1 for v-Se. In order to alleviate a parameter correlation and false minima, ΔE_0 was fixed to be 4.42 eV, which gives the most reasonable bond length of c-Se. The resulting r_1 and σ_1 are tabulated in table 1.

In order to determine the first and second nearest-neighbour distances of c-Se at 80 K, we carried out the Fourier back-transform of $|F(r)|$ in the region which includes both the first and second peaks. The filtered spectrum was fitted with the standard formula based on the three shell model. The intrachain bond length which we obtained is 2.380 Å, nearly the same as that determined from an x-ray diffraction measurement for a single crystal at room temperature by Cherin and Unger [30]. The interchain nearest neighbour and the intrachain second nearest-neighbour distances are 3.38 Å and 3.73 Å, respectively. These are close to the values of 3.436 Å and 3.716 Å obtained from the x-ray diffraction measurement.

Figure 5 shows the temperature variation of bond lengths of c- (open circle) and l-Se (full circle). The bond length decreases with increasing temperature in both crystalline and liquid states, and it is noticed that the bond contracts on melting, while the volume expands. This implies that the intrachain covalent bond is strengthened when the interchain distance increases.

Table 1. The bond length r_1 and the root-mean-square displacement σ_1 for c-, l- and v-Se at various temperatures.

Sample	Temperature (K)	r_1 (Å)	σ_1 (Å)
c-Se	80	2.372	0.044
	300	2.368	0.064
	433	2.362	0.067
	478	2.361	0.069
l-Se	523	2.331	0.072
	573	2.330	0.076
	673	2.327	0.082
	773	2.326	0.089
	873	2.323	0.094
	923	2.322	0.097
v-Se	1473	2.125	0.076

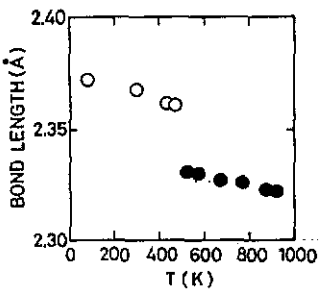

Figure 5. The temperature variation of the Se–Se bond length for c-Se (open circle) and l-Se (full circle).

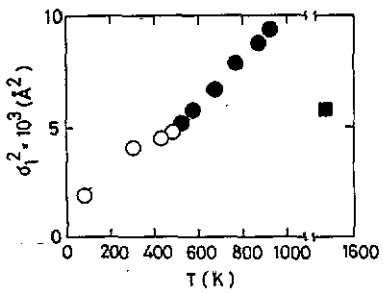

Figure 6. The mean square displacement σ_1^2 of the Se–Se bond length for c-Se (open circle), l-Se (full circle) and v-Se (full square).

The bond length of v-Se deduced from our EXAFS measurement is 2.13 Å, which is slightly shorter than the value of 2.21 Å determined by the electron diffraction measurement by Maxwell and Mosley [31]. The bond length of v-Se is much shorter than that in c- and l-Se.

Figure 6 shows the temperature variation of the mean square displacement σ_1^2 for Se. The values of σ_1^2 for c- (open circle) and l-Se (full circle) become large with increasing temperature, implying that fluctuations in the bond lengths increase owing to the thermal agitation. The value of σ_1^2 for v-Se at 1473 K (full square) is much smaller than that of l-Se near the boiling point.

3.2. Liquid Te

Figure 7 shows $\chi(k)$ for c- and l-Te at various temperatures, including $\chi(k)$ in the supercooled liquid state. The amplitude of $\chi(k)$ for c-Te at 80 K is large in the low k region and has a minimum around 7 Å^{-1} and a maximum around 10 Å^{-1}. Such a variation in the amplitude of $\chi(k)$ corresponds to the k-dependence of the backward scattering amplitude. When the temperature is raised, the oscillation of $\chi(k)$ of c-Te is rapidly damped in the high k region. The EXAFS oscillation is observable even in the liquid state, although the amplitude is much smaller than that in the crystalline state.

Figure 8 shows the magnitude of the Fourier transform, $|F(r)|$, of $k\chi(k)$ for c- and l-Te. In the $|F(r)|$ of c-Te at 80 K the main peak around 2.7 Å can be assigned to the

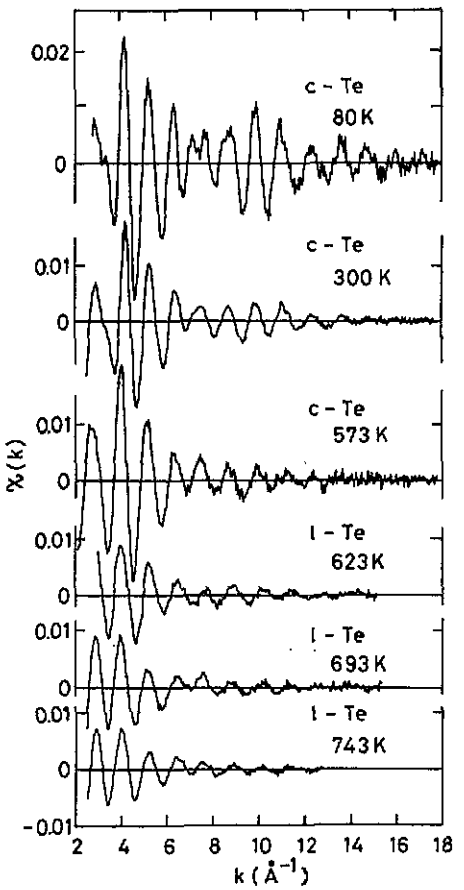

Figure 7. The EXAFS oscillation $\chi(k)$ of c-Te and l-Te at various temperatures including supercooled liquid state. The melting point of Te is 723 K.

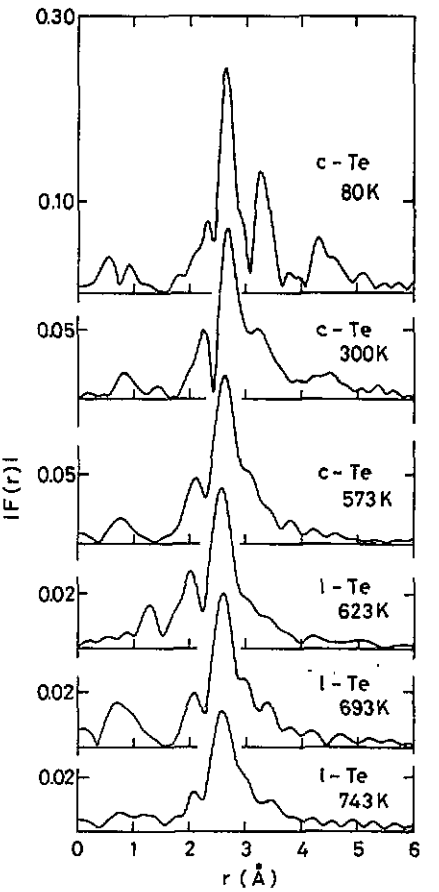

Figure 8. The magnitude of the Fourier transform, $|F(r)|$, of k times $\chi(k)$ in figure 7.

Table 2. The first and second nearest-neighbour distances of c-Te obtained from EXAFS (this work) and x-ray diffraction measurement [33].

	T(K)	r_1(Å)	r_2(Å)
EXAFS	80	2.84	3.48
X-ray diffraction	300	2.835	3.495

intrachain nearest-neighbour distribution. The main peak is split into two, giving a subpeak near 2.3 Å. This arises from the amplitude modulation of $\chi(k)$, which in turn is related to the resonance in the electron–atom scattering processes [32]. The second peak near 3.3 Å gives the distribution of four interchain nearest-neighbour atoms. The third peak around 4.4 Å may be related to the distributions of the intra- and interchain second nearest neighbours. With increasing temperature the second peak is merged into the main peak and the third peak is substantially reduced. The height of the main peak in

Table 3. The first coordination number N_1, the bond length r_1, the interchain nearest-neighbour distance r_2, and the root-mean-square displacement σ_1 for c-Te at various temperatures, obtained from curve fitting using (3).

	T (K)	N_1	r_1 (Å)	σ_1 (Å)	r_2 (Å)
c-Te	80	1.93	2.84	0.019	3.47
	300	2.00	2.83	0.063	—
	573	1.86	2.83	0.072	—

Table 4. The first coordination number N_1, the bond length r_1, and the root-mean-square displacement σ_1 for l-Te at various temperatures, obtained from curve fitting using (3) on the assumption that $G(r)$ consists of one Gaussian curve.

T(K)	N_1	r_1 (Å)	σ_1 (Å)	
l-Te	623	0.94	2.79	0.067
	673	0.84	2.79	0.076
	693	0.81	2.79	0.067
	713	0.79	2.78	0.070
	743	0.76	2.80	0.083
	773	0.82	2.87	0.103

the liquid state is reduced to half of that in the crystalline state; this is in contrast to the results for Se. The main peak of l-Te has a tail extending to larger spacing and its position is shifted to smaller spacing on melting.

The first and second peaks in $|F(r)|$ for c-Te were Fourier back transformed. This filtered $\tilde{\chi}(k)$ spectrum was fitted with the standard formula based on a two shell model to determine the intra- and interchain nearest-neighbour distances. The resulting bond length for c-Te at 80 K is 2.84 Å; this is much larger than that for c-Se. In table 2 our values of the intrachain nearest-neighbour distance r_1 and interchain nearest-neighbour distance r_2 are compared with the data determined by the x-ray diffraction measurement for a single crystal at room temperature [33].

Since the main peak becomes broader and the second peak merges into the main peak at high temperatures, the standard formula may no longer be appropriate for fitting the EXAFS spectrum. In the present analysis the following formula was used.

$$k^2\tilde{\chi}(k) = SB_{\mathrm{Te}}(k')k' \int \mathrm{d}r\, 4\pi\rho_0 r^2 G(r) \frac{\sin(2k'r + \varphi_{\mathrm{Te}}(k'))}{r^2} \tag{3}$$

where it is assumed that pair distribution function $G(r)$ is expressed by the superposition of Gaussian curves as given by (4).

$$G(r) = \sum_i \frac{N_i}{\sqrt{2\pi}\sigma_i} \exp\left(-\frac{(r-r_i)^2}{2\sigma_i^2}\right). \tag{4}$$

The number density ρ_0 was taken from the data by Thurn and Ruska [8]. The value of ΔE_0 was fixed to be -0.90 eV; this was obtained by fitting $\chi(k)$ of c-Te at 80 K with the standard formula. The value of S was selected to be 0.097, giving 2 as the coordination number of c-Te. The curve fitting was carried out assuming that $G(r)$ consists of two Gaussians. The resulting intrachain nearest-neighbour distance r_1, coordination number

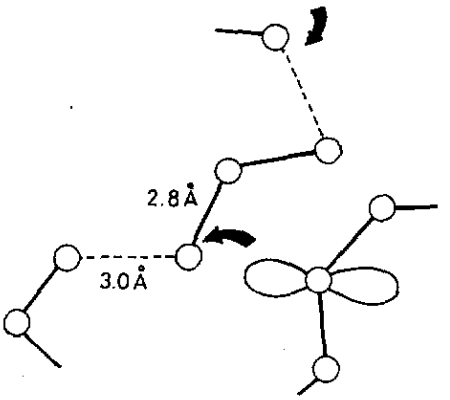

Figure 9. Schematic diagram of l-Te consisting of chain molecules with shorter and longer bonds. The charge transfer from the lone pair orbital in the neighbouring chain may result in weakening the covalent bond.

Table 5. The coordination number N, the bond length r and the root-mean-square displacement σ for shorter and longer bonds in l-Te at various temperatures obtained from curve fitting using (3) on the assumption that $G(r)$ consists of two Gaussian peaks.

		Shorter bond			Longer bond		
	T(K)	N	r(Å)	σ(Å)	N	r(Å)	σ(Å)
l-Te	623	0.94	2.78	0.064	1.06	2.97	0.154
	673	0.98	2.78	0.080	1.02	3.03	0.200
	693	0.65	2.78	0.056	1.35	2.93	0.185
	713	0.59	2.77	0.055	1.41	2.92	0.173
	743	0.69	2.79	0.077	1.31	2.96	0.224
	773	0.65	2.83	0.076	1.35	3.04	0.188

N_1 and mean square displacement σ_1 for c-Te are listed in table 3. The bond length of c-Te was found to be 2.84 Å at 80 K, which is in agreement with the result of the standard fitting method, and it changes little with increasing temperature. The interchain nearest-neighbour distance r_2 is 3.47 Å at 80 K. Unfortunately we cannot determine r_2 accurately at higher temperatures.

The curve fitting for l-Te is carried out on the assumption that $G(r)$ consists of only one Gaussian. Table 4 shows the structural parameters of l-Te at various temperatures. As seen in table 4, we obtain about 1 for the coordination number of l-Te. It is, however, unreasonable to expect that l-Te might consist of dimers as in the vapour phase.

Recent neutron diffraction measurements [5, 6] show that the two-fold coordinated structure of Te is preserved even in the liquid state. The ratio of r_1 to r_2 in c-Te is larger than in c-Se, suggesting that the interchain coupling is rather strong in Te. At high temperatures the thermal motion of atoms becomes violent and an atom can approach very close to another atom in the neighbouring chain. The charge transfer from the occupied lone pair orbital to the unoccupied antibonding orbital in the adjacent chain is thereby enhanced. This charge transfer from the neighbouring chain may also result in a weakening of the covalent bond. Hence we suppose that the chain structure of l-Te is formed by at least two kinds of covalent bonds: shorter and longer ones as shown in figure 9. It is reasonable to consider that the EXAFS signal from the atoms in the neighbouring chains is substantially damped by disorder and thermal agitation in the liquid state. Therefore, we performed the curve fitting, assuming that $G(r)$ within the

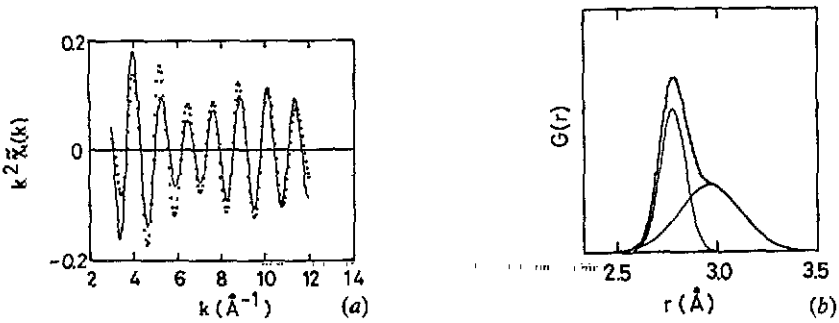

Figure 10. (*a*) Comparison of the theoretical fit (solid curve) with the Fourier filtered spectrum of l-Te at 623 K (dotted curve). (*b*) $G(r)$ used for the theoretical fit in figure 10(*a*).

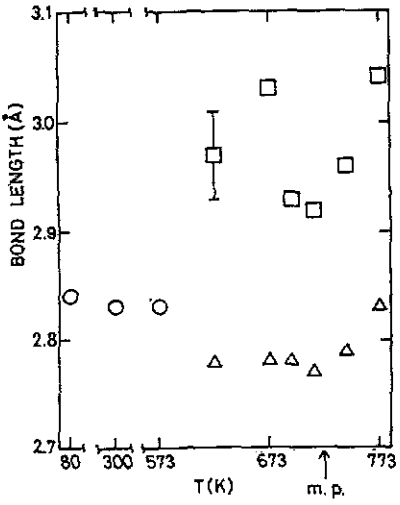

Figure 11. The temperature variation of the shorter (triangle) and longer (square) bond lengths for l-Te. Circles denote the intrachain bond length of c-Te, obtained from curve fitting, on the assumption that $G(r)$ consists of two Gaussians.

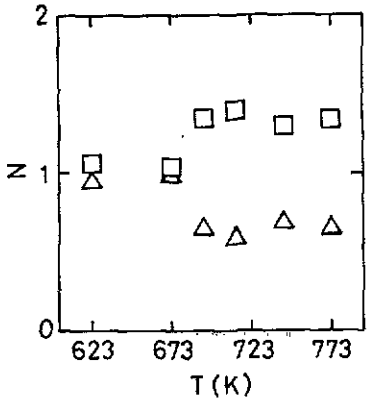

Figure 12. The temperature variation of the average number N of the shorter (triangle) and longer (square) bonds per atom in l-Te.

chain consists of two Gaussians and that the total coordination number is 2. The refined structural parameters are listed in table 5.

The bond lengths of l-Te at 623 K are given as 2.78 Å and 2.97 Å. The shorter bond length is almost the same as that estimated from the one-Gaussian fitting. It is observed that the longer bond is much shorter than the interchain nearest-neighbour distance in c-Te. In figure 10(*a*) the theoretical fit using (3) is shown by a solid curve; for comparison, the Fourier filtered spectrum of l-Te at 623 K is denoted by a dotted curve. As seen in the figure, the agreement is satisfactory. In figure 10(*b*) we show the $G(r)$ used for the theoretical fit. The temperature variation of the shorter (triangle) and longer (square) bond lengths are shown in figure 11. The bonds elongate slightly with increasing temperature. The average numbers of the shorter (triangle) and longer (square) bonds per atom are plotted as a function of temperature in figure 12. The longer bond is more probable than the shorter one above 690 K.

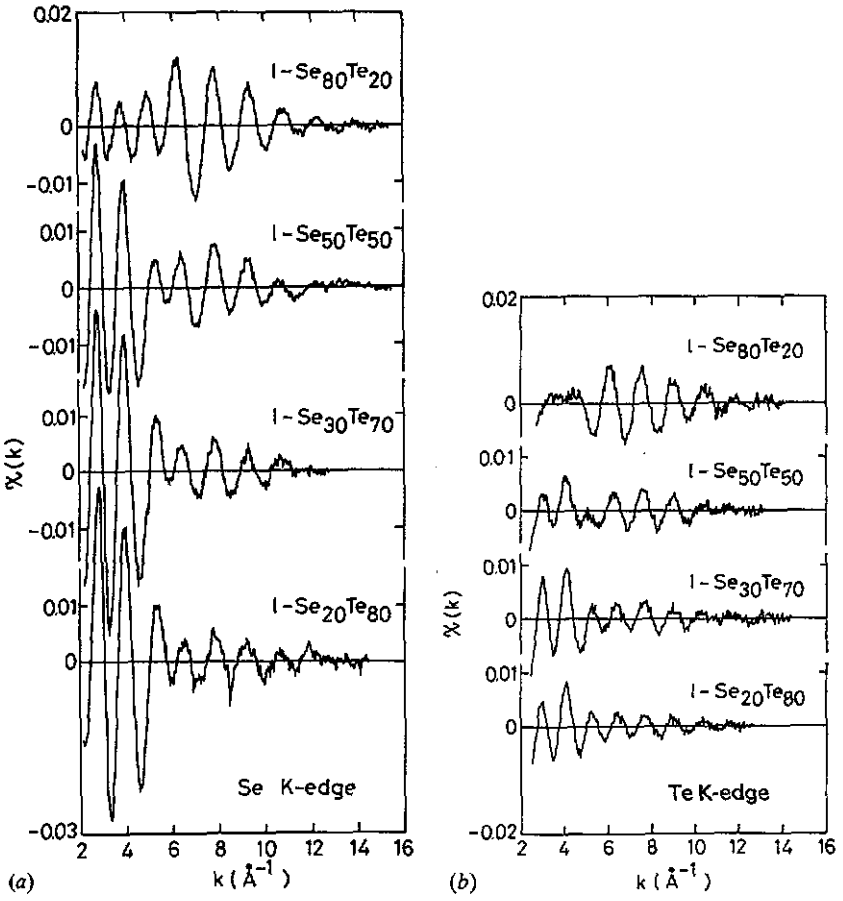

Figure 13. (*a*) The EXAFS oscillation $\chi(k)$ taken on the Se K-edge for l-$Se_{80}Te_{20}$ at 573 K, l-$Se_{50}Te_{50}$ at 673 K, l-$Se_{30}Te_{70}$ and $Se_{20}Te_{80}$ at 723 K. (*b*) The EXAFS oscillation $\chi(k)$ taken on the Te K-edge for the data in (*a*).

Many investigators have proposed the existence of a three-fold site with an As-like pyrimidal configuration in l-Te. However, the present EXAFS study has given no evidence for the pyramidal configuration.

3.3. Liquid Se–Te mixtures

Figure 13(*a*) shows $\chi(k)$ taken on the Se K-edge of l-$Se_{80}Te_{20}$ at 573 K, $Se_{50}Te_{50}$ at 673 K, $Se_{30}Te_{70}$ and $Se_{20}Te_{80}$ at 723 K. The amplitude of $\chi(k)$ of l-$Se_{80}Te_{20}$ has a peak around 7 $Å^{-1}$, as was seen in pure l-Se. With increasing Te concentration the amplitude becomes considerably larger in the low k region. This is owing to the strong backward scattering from Te atoms around a central Se atom. Figure 13(*b*) shows $\chi(k)$ above the Te K-edge of these liquid Se–Te mixtures. The amplitude of the oscillation is small compared with that for the Se K-edge.

Figure 14(*a*) shows the Fourier transform, $|F(r)|$, of k times $\chi(k)$, taken from figure 13(*a*). There exists only a main peak, which corresponds to the distribution of the nearest-neighbour atoms around a central Se atom. In the $|F(r)|$ of l-$Se_{80}Te_{20}$ the shape

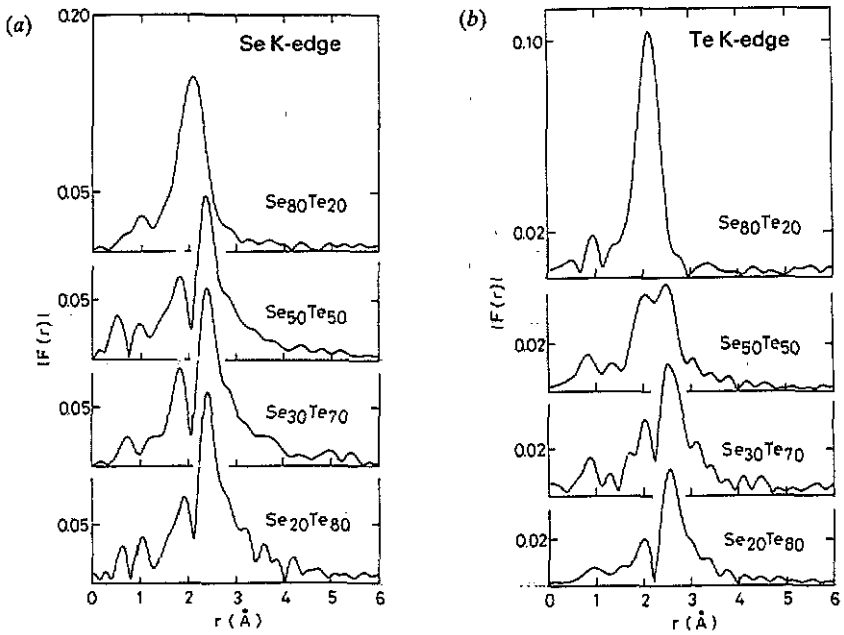

Figure 14. (*a*) The magnitude of the Fourier transform, $|F(r)|$, of k times $\chi(k)$ in figure 13(*a*). (*b*) The magnitude of the Fourier transform, $|F(r)|$, of k times $\chi(k)$ in figure 13(*b*).

of the main peak is similar to that of l-Se, implying that most of neighbouring atoms are Se atoms. In $|F(r)|$ at 50% or more Te concentration, the main peak splits into two and there appears a sharp minimum around 2 Å. The results of the curve fitting analysis show that this minimum comes from the interference effect between the EXAFS signals from neighbouring Se and Te atoms. Figure 14(*b*) shows the Fourier transform, $|F(r)|$, of k times $\chi(k)$, taken from figure 13(*b*). The first peak of l-$Se_{80}Te_{20}$ is sharp. The main peaks of l-$Se_{50}Te_{50}$, l-$Se_{30}Te_{70}$ and $Se_{20}Te_{80}$ have a minimum around 2.2 Å.

Large differences in k-dependence of the backward scattering amplitude and phase shift functions between Se and Te atoms make it possible to separate the partial distributions. In order to obtain partial distributions of Se(Se–Se) and Te(Se–Te) around a central Se atom (Se), and Te(Te–Te) and Se(Te–Se) around a central Te atom (Te), we performed the following curve fitting analysis. The main peaks in $|F(r)|$ for Se and Te K-edges were backtransformed into k-space. Since the partial distribution of Se–Te must be the same as that of Te–Se, both the filtered spectra were simultaneously fitted with the following equations.

$$k_i^2\chi(k_i) = S_i \sum_j B_j(k_{ij})k_{ij} \int \mathrm{d}r\, 4\pi\rho_0 r^2 G_i(r) \frac{\sin(2k_{ij}r + \varphi_{ij}(k_{ij}))}{r^2} \tag{5}$$

$$G_i(r) = \sum_j \frac{N_{ij}}{\sqrt{2\pi}\sigma_{ij}} \exp\left(-\frac{(r - r_{ij})^2}{2\sigma_{ij}^2}\right) \tag{6}$$

$$k_{ij} = (k_i^2 - \Delta E_{0ij}/3.81)^{1/2}. \tag{7}$$

Here i and j denote Se and Te, r_{ij} the bond length, N_{ij} the partial coordination number and σ_{ij} the mean square displacement of the bond length between a central atom i and a neighbouring atom j. The scaling factor S_{Te} is the same value as S of l-Te. The value of

S_{Se} was selected to be 0.29, so that the coordination number of c-Se would be 2. The values of ΔE_{0SeSe} and ΔE_{0TeTe} were fixed to be those of l-Se and l-Te. The condition that the partial distribution of Se–Te should be the same as that of Te–Se was expressed as $r_{SeTe} = r_{TeSe}$, $\sigma_{SeTe} = \sigma_{TeSe}$ and $c_{Se}N_{SeTe} = c_{Te}N_{TeSe}$, where c_i denotes the concentration of an i-element. We first tried to fit the spectra with (5)–(7), assuming that the coordination number of Se and Te atoms was fixed to be 2 in the mixtures. As discussed in the previous section, the strong interchain coupling in l-Te weakens the intrachain bond, resulting in the appearance of shorter and longer bonds. In order to reproduce the filtered spectra of the Te K-edge for the Se–Te mixtures by using (5)–(7), it was necessary to introduce two kinds of Te–Te bonds. The resulting bond lengths, partial coordination numbers and the mean square displacements are listed in table 6. We cannot obtain reasonable values of parameters for the Te–Te bonds of l-$Se_{80}Te_{20}$ because the contribution of the Te–Te bonds to the EXAFS oscillation is too small.

Figure 15 shows the Se–Se (circle), Se–Te (diamond), shorter (triangle) and longer (square) Te–Te bond lengths at 773 K as a function of Te content x. The Se–Se bond elongates with increasing Te concentration. We suggest that this elongation is caused by the intra- and interchain charge transfer from an occupied lone pair orbital of a Te atom to an unoccupied antibonding orbital of the neighbouring Se–Se bond, because the ionization potential of Te is higher than that of an Se atom. The Se–Te bond and the shorter Te–Te bond lengthen slightly with increasing Te content.

Figure 16 shows the probabilities that Te atoms are distributed around a central Se atom (circle) and a central Te atom (square) as a function of Te content x. These are deduced from the evaluation of the partial coordination numbers at 773 K. With increasing Te concentration each of the probabilities becomes large, approaching 1 almost linearly; this suggests that the Se and Te atoms are arranged at random in a chain molecule.

In figure 17 the average number N^{L}_{Te-Te} of Te atoms which lie at a longer distance (square) from a central Te atom is shown as a function of temperature for l-$Se_{50}Te_{50}$, $Se_{30}Te_{70}$ and $Se_{20}Te_{80}$. For l-$Se_{50}Te_{50}$ N^{L}_{Te-Te} is about 0.5 at 673 K and increases slightly with temperature. For the liquid mixtures with high Te content N^{L}_{Te-Te} increases remarkably with temperature. The value of N^{L}_{Te-Te} for l-$Se_{20}Te_{80}$ at 873 K reaches about 1.3, which is nearly the same as that for l-Te. The charge transfer between neighbouring chains leads to the electron delocalization around Te atoms, resulting in the elongation of Te–Te bonds. This may be enhanced when the temperature or the Te content is increased. Our previous NMR study suggests that the electrons around Te sites in the chain tend to be delocalized, but this is not the case around Se sites [19]. It is concluded that the rapid increase in N^{L}_{Te-Te} is associated with the semiconductor-to-metal transition.

4. Summary

We have measured EXAFS of l-Se, Te, Se–Te mixtures and v-Se for the first time, using a sample cell of our own design. It was found that the intrachain bond becomes strong when the interchain distance increases and the interchain coupling is reduced. The EXAFS spectra of l-Te could be reproduced well by assuming a two-fold coordinated chain structure with shorter and longer bonds within the chain. Their lengths are 2.78 Å and 2.97 Å at 623 K in the supercooled liquid state. The longer bond is preferable as temperature is raised.

In order to obtain partial structure parameters in liquid Se–Te mixtures, the filtered spectra measured on both of the Se and Te K-edges were simultaneously fitted assuming

Table 6. The coordination number N, the bond length r and the root-mean-square displacement σ for Se–Se, Se–Te, Te–Se and shorter and longer Te–Te bonds in liquid Se–Te mixtures at various temperatures. Here the element on the left side of the hyphen is defined as the central atom.

		Se–Se			Se–Te			Te–Se			Te–Te					
											Shorter bond			Longer bond		
	T(K)	N	r(Å)	σ(Å)	N	r(Å)	σ(Å)	N	r(Å)	σ(Å)	N	r(Å)	σ(Å)	N	r(Å)	σ(Å)
$Se_{80}Te_{20}$	573	1.54	2.33	0.073	0.46	2.54	0.055	1.85	2.54	0.055						
	673	1.59	2.33	0.083	0.41	2.53	0.058	1.62	2.53	0.058						
	773	1.63	2.33	0.093	0.37	2.51	0.058	1.48	2.51	0.058						
$Se_{50}Te_{50}$	673	1.11	2.34	0.065	0.89	2.53	0.077	0.89	2.53	0.077	0.58	2.75	0.044	0.53	2.97	0.154
	773	1.13	2.34	0.098	0.87	2.53	0.088	0.87	2.53	0.088	0.54	2.75	0.055	0.58	2.98	0.167
	873	1.15	2.35	0.104	0.85	2.52	0.095	0.85	2.52	0.095	0.54	2.75	0.079	0.61	2.97	0.190
$Se_{30}Te_{70}$	723	0.83	2.36	0.098	1.17	2.53	0.090	0.50	2.53	0.090	1.06	2.74	0.063	0.44	2.92	0.176
	773	0.83	2.36	0.101	1.17	2.53	0.097	0.50	2.53	0.097	0.82	2.75	0.066	0.68	2.93	0.195
	873	1.04	2.36	0.124	0.96	2.52	0.095	0.41	2.52	0.095	0.74	2.75	0.081	0.84	2.96	0.204
$Se_{20}Te_{80}$	723	0.92	2.38	0.132	1.08	2.55	0.081	0.27	2.55	0.081	0.81	2.76	0.070	0.92	2.97	0.194
	773	1.01	2.41	0.135	0.99	2.53	0.085	0.25	2.53	0.085	0.51	2.75	0.058	1.25	2.96	0.202
	873	1.14	2.42	0.157	0.86	2.54	0.089	0.21	2.54	0.089	0.50	2.80	0.079	1.29	3.28	0.313

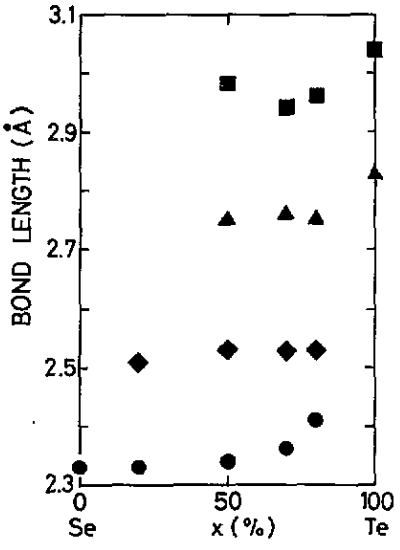

Figure 15. The Se–Se (circle), Se–Te (diamond), shorter Te–Te (triangle) and longer Te–Te (square) bond lengths of liquid Se–Te mixtures as a function of Te content x.

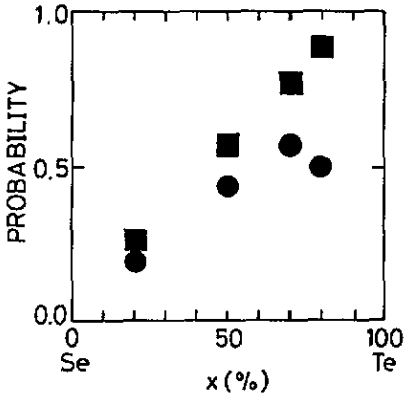

Figure 16. The probabilities that Te atoms are distributed around a central Se atom (circle) and a central Te atom (square) as a function of Te content x.

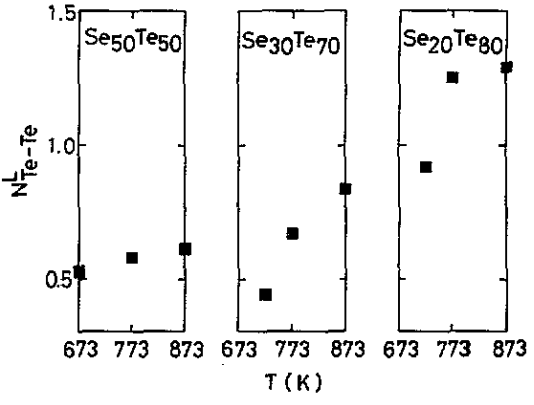

Figure 17. The temperature variation of the average number of Te atoms around a central Te atom at a longer distance for l-$Se_{50}Te_{50}$, $Se_{30}Te_{70}$ and $Se_{20}Te_{80}$.

a two-fold coordinated structure. By postulating the existence of shorter and longer Te–Te bonds, the spectra taken on the Te K-edge were reproduced better. The number of longer Te–Te bonds increases with increasing temperature or increasing Te concentration. This may be associated with the semiconductor-to-metal transition.

Acknowledgments

The authors would like to thank Professor M Nomura and Mr A Koyama for their valuable discussions. This work was partly supported by the Grant-in-Aid for Scientific Research Fund from the Ministry of Education, Science and Culture of Japan.

References

[1] Tourand G 1973 *J. Physiq.* **34** 934
[2] Misawa M and Suzuki K 1977 *Trans. JIM* **18** 427
[3] Tourand G and Breuil M 1972 *J. Physiq.* **32** 813
[4] Waseda Y and Tamaki S 1975 *Z. Naturforsch.* **30A** 1655
[5] Takeda S, Tamaki S and Waseda Y 1984 *J. Phys. Soc. Japan* **53** 3830
[6] Menelle A, Bellissent R and Flank A M 1989 *Physica* B **156/157** 174
[7] Enderby J E and Barnes A C 1990 *Rep. Prog. Phys.* **53** 85
[8] Thurn H and Ruska J 1976 *J. Non-Cryst. Solids* **22** 331
[9] Hoshino H and Endo H 1987 *J. Phys. Soc. Japan* **56** 225
[10] Yao M, Suzuki K and Endo H 1980 *Solid State Commun.* **34** 187
[11] Takimoto K and Endo H 1982 *Phys. Chem. Liquids* **12** 141
[12] Takeda S, Okazaki H and Tamaki S 1985 *J. Phys. Soc. Japan* **54** 1890
[13] Perron J C 1967 *Adv. Phys.* **16** 657
[14] Yao M, Misonou M, Tamura K, Ishida K, Tsuji K and Endo H 1980 *J. Phys. Soc. Japan* **48** 109
[15] Endo H 1984 *J. Non-Cryst. Solids* **61/62** 1
[16] Freyland W and Cutler M 1980 *J. Chem. Soc. Faraday II* **76** 756
[17] Gardner J A and Cutler M 1976 *Phys. Rev.* B **14** 4488
[18] Warren Jr W W and Dupree R 1980 *Phys. Rev.* B **22** 2257
[19] Misonou M and Endo H 1982 *J. Phys. Soc. Japan* **51** 2285
[20] Seyer H-P, Tamura K, Hoshino H, Endo H and Hensel F 1986 *Ber. Bunsenges. Phys. Chem.* **90** 587
[21] Silva L A and Cutler M 1990 *Phys. Rev.* B **42** 7103
[22] Crozier E D, Lytle F W, Sayers D E and Stern A 1977 *Can. J. Chem.* **55** 1968
[23] Crozier E D and Seary A J 1980 *Can. J. Phys.* **58** 1388
[24] Orton B R, Malra G K and Steel A T 1987 *J. Phys. F: Met. Phys.* **17** 145
[25] Inui M, Tamura K, Yao M, Endo H, Hosokawa S and Hoshino H 1990 *J. Non-Cryst. Solids* **117/118** 112
[26] Nomura M and Koyama A 1989 KEK Report 89-16; 1991 *X-ray Absorption Fine Structure* ed SS Hasnain (London: Ellis Horwood) pp 667–9
[27] Inui M, Yao M and Endo H 1988 *J. Phys. Soc. Japan* **57** 553
[28] Rau H 1974 *J. Chem. Thermodynamics* **6** 525
[29] McKale A G, Veal B W, Paulikans A P, Chan S-K and Knapp G S 1988 *J. Am. Chem. Soc.* **110** 3763
[30] Cherin P and Unger P 1967 *Inorg. Chem.* **6** 1589
[31] Maxwell L R and Mosley V M 1939 *Phys. Rev.* **55** 238
[32] Teo B-K and Lee P A 1979 *J. Am. Chem. Soc.* **101** 2815
[33] Cherin P and Unger P 1967 *Acta Crystallogr.* **23** 670